Journal of Industrial and Engineering Chemistry 22 (2015) 120–126

Contents lists available at ScienceDirect

Journal of Industrial and Engineering Chemistry

journal homepage: www.elsevier.com/locate/jiec

Ink-jetting and rheological behavior of a silica particle suspension

Wen Ling Zhang [a], Hyoung Jin Choi [a,*], Hyun-Seok Ko [b], Kye-Si Kwon [c]

[a] Department of Polymer Science and Engineering, Inha University, Incheon 402-751, South Korea
[b] Department of Electrical & Robot Engineering, Soonchunhyang University, Asan, 336-745, South Korea
[c] Department of Mechanical Engineering, Soonchunhyang University, Asan, 336-745, South Korea

ARTICLE INFO

Article history:
Received 21 May 2014
Received in revised form 10 June 2014
Accepted 13 June 2014
Available online 2 July 2014

Keywords:
Silica particle
Suspension
Rheology
Ink-jetting

ABSTRACT

To understand the particle-suspended inkjet behavior better, silica particle solutions with different particle sizes were dispersed in ethylene glycol. The effects of the particle size on the jetting behavior was examined using a laboratory-developed drop watcher system in addition to their rheological properties determined using a rotational rheometer. The drying characteristics of the silica solutions with different particle sizes on a glass substrate were also investigated. The results revealed a similar size of deposition droplets after the evaporation of droplets at 5 wt%, whereas a smaller deposition size was observed at 1 wt%.

Introduction

The application of ink-jet printing technology is broadening from a home printer to the electronic industry because of its inexpensive manufacturing and production cost compared to conventional manufacturing technologies [1–4]. The potential applications of ink-jet printing in engineering include printed circuit boards, textile products, color filters for thin-film transistors in the liquid crystal display, sensor fabrication and radio frequency identification [5–9]. On the other hand, it is crucial to optimize the jetting parameters to ensure that the printing process is error-free. The jetting characteristics, such as the jetting speed, ligament and satellites, as well as the morphological characteristics of the jetted droplet on a substrate should meet the requirements for various commercial applications [10,11]. The performance of ink-jet printing depends on the ink properties and other factors [12]. To understand the mechanism of the ink drop process more clearly, it is important to study the intrinsic characteristics of the inks, such as the rheological properties (shear viscosity and storage modulus), surface tension and evaporation characteristics. [13]. In particular, the rheological characteristics of the inks are critical due to the requirements from the jet stability and printed pattern uniformity after drying on the substrates.

In general, an ink-jet ink is composed of the appropriate portion of dispersant, functional particles and suspending medium [13]. Polymer solutions with an appropriate polymer concentration and molecular weights are also used as ink-jet inks [14,15]. Wang et al. [16] reported the ink-jet properties of a modified SiO_2 sol. Later, the different ink-jet properties between pure nano-SiO_2 and modified nano-SiO_2 with a silica coupling agent were studied [12]. The present study examined the ink-jetting behavior and drying characteristics of the silica particle solutions with different sizes from nanoparticles to mono-dispersed microspheres.

Experimental

Materials

Silica particles with different particle sizes (80 nm, 0.5 μm, 1.0 μm and 1.5 μm, obtained from Alfa Aesar) were dispersed in ethylene glycol (EG) (AMRESCO, high purity grade) by sonication for 1 h to obtain a homogeneous suspension of each particle size with two different (1 and 5 wt%) particle concentrations.

Rheological measurements

The rheological properties of the silica particle-dispersed suspensions were examined using a rotational rheometer (MCR 300, Anton Paar) equipped with a double Couette cylindrical system [DG 26.7 (the diameter of the cup was 27.59/23.83 mm and the diameter of the bob was 26.66/24.66 mm)/TEZ 150 P-C] at room temperature [17].

* Corresponding author. Tel.: +82 328607486.
E-mail address: hjchoi@inha.ac.kr (H.J. Choi).

http://dx.doi.org/10.1016/j.jiec.2014.06.032
1226-086X/

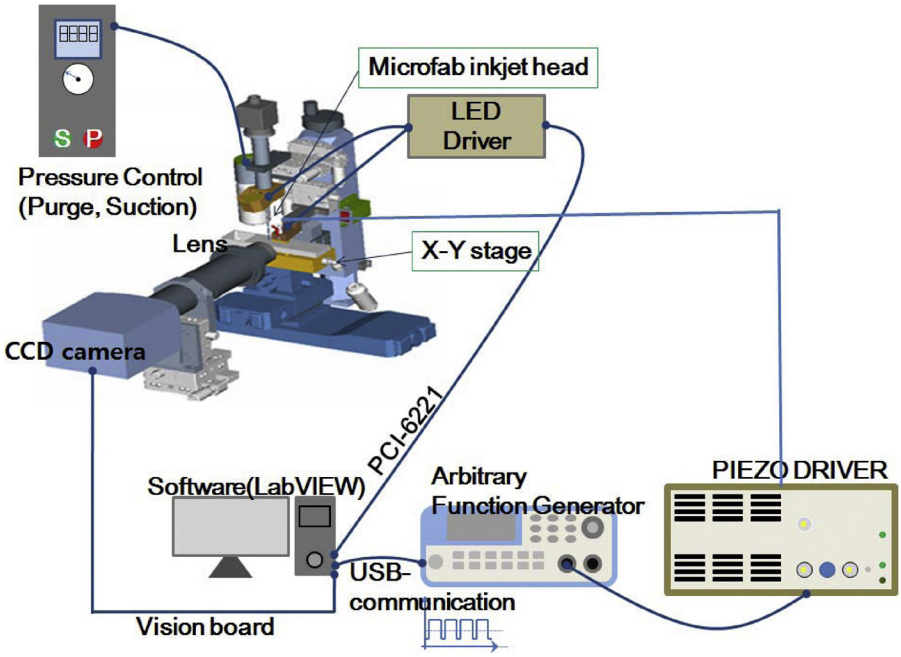

Fig. 1. Equipment for jetting and drying characterization—schematic of drop watcher system.

Measurement of the ink-jetting behavior

A laboratory-developed drop watcher system shown in Fig. 1 was used to characterize the jet. A single nozzle head (MJ-AT, Microfab, USA) was used as the jetting device. The nozzle diameter of the print-head used for the experiment was 50 μm. A CCD camera (XC ES 50, Sony, Japan) was used to obtain jetting images. An adjustable zoom lens (ML-Z07545, MORITEX, Japan) and a lens adaptor (ML-Z20, MORITEX, Japan) were used to acquire magnified images of the ink-jet behavior. To obtain a frozen jetting image, LED light was synchronized with respect to the jet triggers.

Two digital pulse trains from a counter board (PCI-6221, NI, USA) were used for the synchronization, as shown in Fig. 2. The first digital pulse train was used as a trigger signal to create the pulse voltage, whereas the second pulse train was exploited to control the LED light. The second pulse was triggered from the first pulse, and the trigger delay time between the first and second pulse was adjusted, such that the jet image at the delayed time can appear frozen [18]. In addition, it can be also noted that pure EG behavior was previously studied [18], in which the ligament of jetted pure EG tends to become spherical without forming satellites. However, the long ligament of jetted particle solution ink was likely to break into many satellites during drop formation.

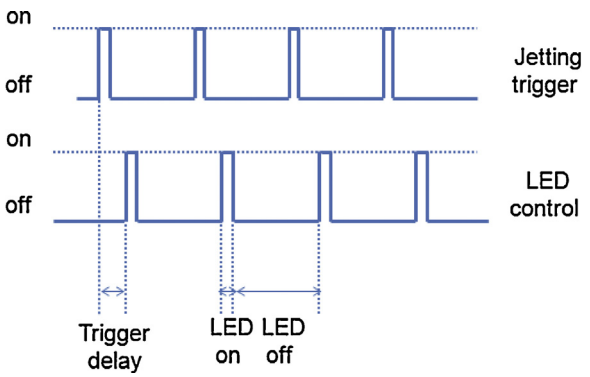

Fig. 2. Strobe LED control.

Measurement of drying behavior

The drop watcher system presented in Fig. 1 was also equipped with a substrate holder. As a result, the drying behavior of the droplet on a substrate can be measured by lowering the LED and camera position slightly downward to align the jetted droplet on the substrate with respect to the camera. Fig. 3 shows the droplet image from the side and top views after jetting on a substrate.

Unlike the drop watcher system for jetting visualization, the LED light should not be synchronized with respect to jetting when observing the drying behavior. For this purpose, the counter board was re-configured such that the LED light can be controlled

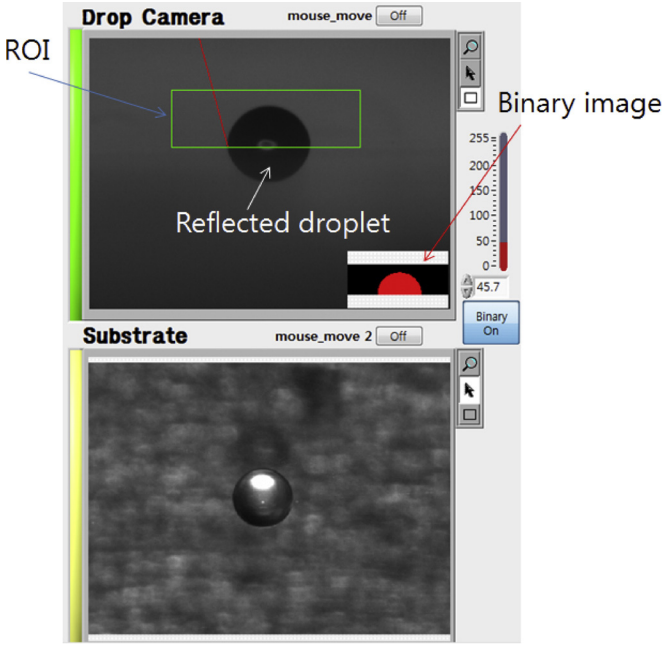

Fig. 3. Side view and top view after jetting.

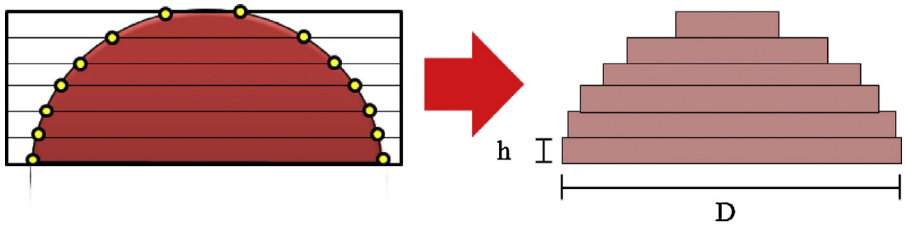

(a) Droplet volume measurement algorithm

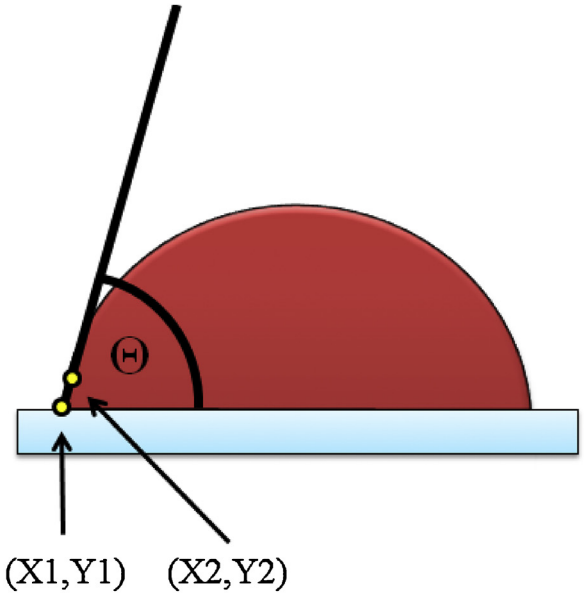

(b) Contact angle measurement based on edge profile

Fig. 4. Droplet measurement based on edge detection.

independently with respect to the jetting signal to provide sufficient light intensity to acquire droplet images on the substrate.

The droplet volume on the substrate can be controlled easily by setting the ink-jetting droplet number. For example, if 25 droplets are used, the droplet volume can be approximately 2 nL. Note that the droplet volume of one droplet is approximately 80 pL. In addition, because the 25 droplets were placed on the substrate with 1 kHz jetting frequency, the deposition time of 25 droplets was about 25 ms. The images for the drying process were then captured and saved at the user-defined timing intervals. The captured images were examined further to understand the drying behavior of the droplet on the substrate.

From the side view of a droplet, an edge detection based algorithm was developed to extract its side view droplet profile. To analyze the droplet efficiently, the region of interest (ROI) was defined around the droplet on the substrate to specify the image analysis area. In the two-dimensional ROI, predetermined horizontal-line ROIs was defined to detect the edges, which have information about the droplet profile. The droplet volume could be calculated from the two dimensional droplet profile assuming a 3-D droplet shape. For example, if the droplet is considered to be axis-symmetric with respect to its center, the volume can be calculated by the summation of sliced cylinders, as shown in Fig. 4(a). Here, the diameter of the sliced cylinder can be identified by the horizontal length of two detected edges, whereas the height of the cylinder is equal to the spacing between the horizontal-line ROIs. Note that the accuracy of the measured droplet volume can decrease when the droplet becomes smaller due to the image resolution, making it difficult to calculate the volume of the remaining solid contents after evaporation.

The contact angle can also be calculated using two detected edges near the interface between the droplet and surface, as shown in Fig. 4 (b).

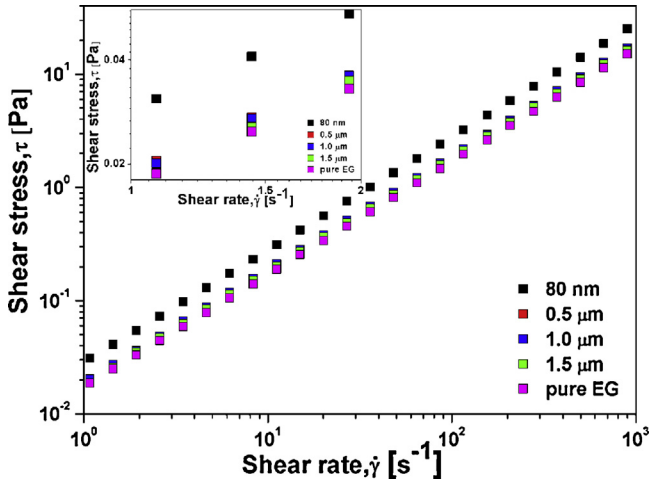

Fig. 5. Shear stress as a function of shear rate for silica particle solutions with different particle size (5 wt%, particle concentration, the inset is the enlarged part at shear rate range from 1 to 2 1/s).

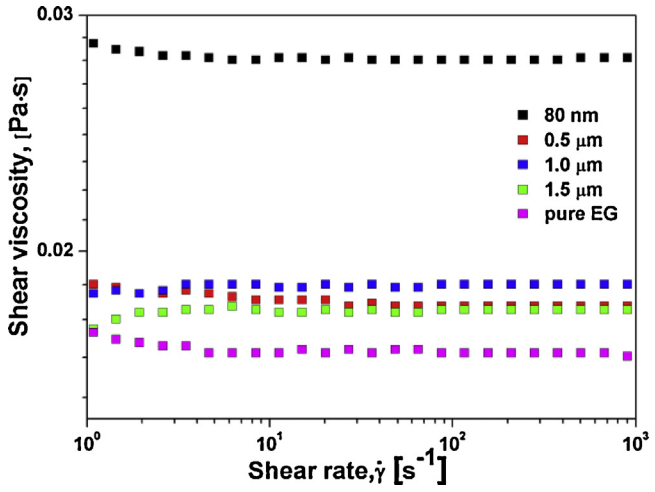

Fig. 6. Shear viscosity as a function of shear rate for silica particle solutions with different particle size (5 wt%, particle concentration).

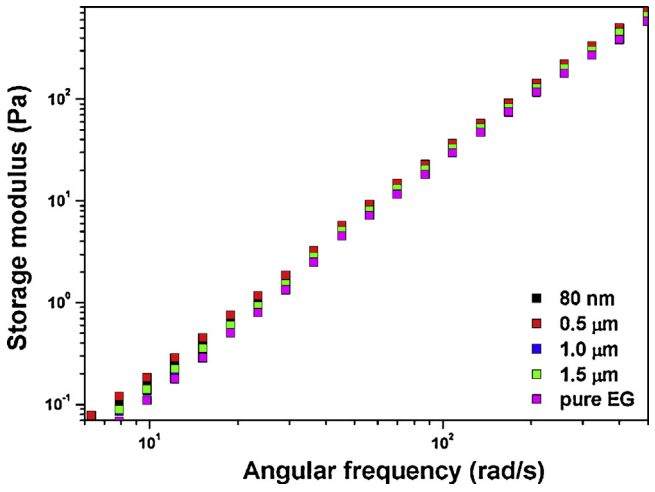

Fig. 7. Angular frequency sweep for silica particle solutions with different particle size (5 wt%, particle concentration).

Results and Discussion

The density of the silica nanoparticle (80 nm) and silica microsphere (0.5 μm, 1.0 μm and 1.5 μm) used were approximately 2.2–2.6 g/cm^3 and 2.0 g/cm^3, respectively. The particle solution becomes transparent with decreasing particle size due to the improved refractive index match and dispersibility.

The structure of the ink material may be subject to an abrupt transition during the ink-jet process. Therefore, their rheological properties should be examined using steady shear or dynamic tests [4,19–21]. Their rheological properties were examined using a rotational rheometer. For all silica particle solutions, the shear stress increased linearly with increasing shear rate, showing typical Newtonian fluid behavior, as shown in Fig. 5. In addition, the silica microsphere solutions (0.5 μm, 1.0 μm and 1.5 μm) exhibited similar shear stresses, which is slightly lower than that of the nano-silica solution (80 nm). The particle size with a nanoscale might increase the adjacent particle interactions during the shearing process, which generates high shear stress.

As shown in Fig. 6, Newtonian fluid-like properties can be found in all silica particle solutions, in which the shear viscosity is uniform with the applied shear rate. A silica solution with an 80 nm particle size shows the highest shear viscosity among the sample solutions, which agrees with the trend in the shear stress.

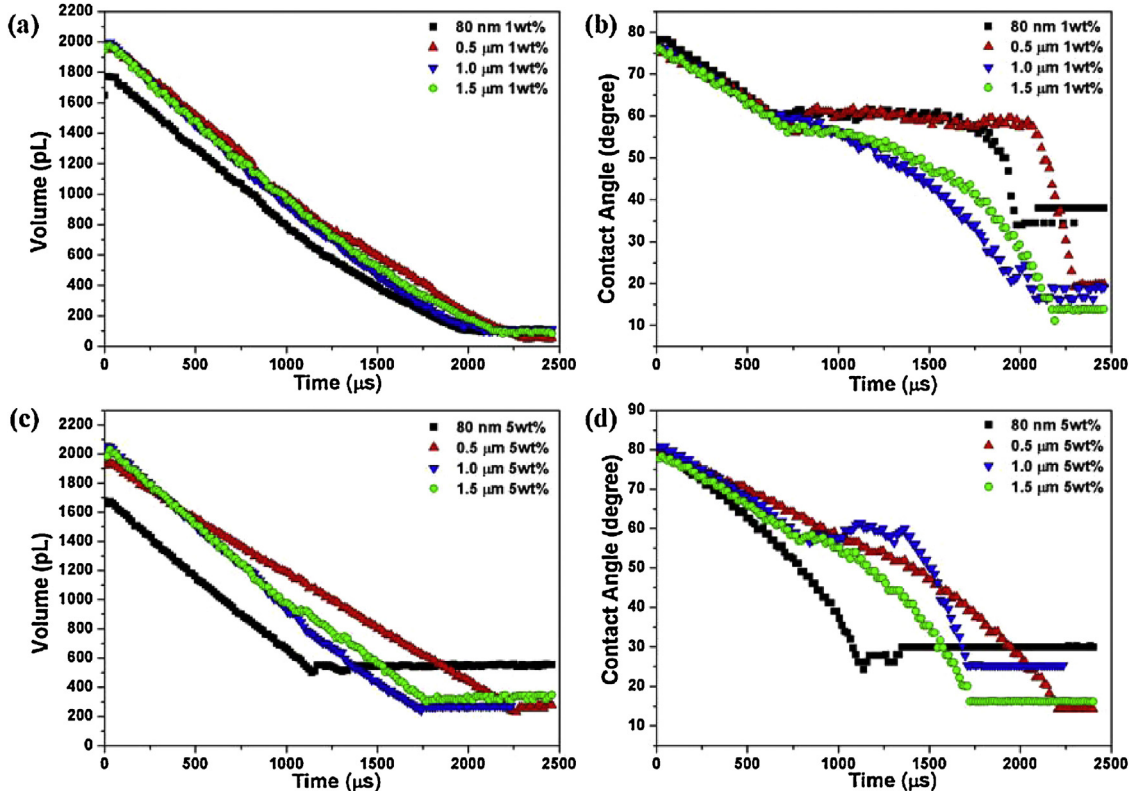

Fig. 8. Drop volume (a, c) and contact angle (b, d) of silica particle solutions (1 and 5 wt%, particle concentration) with different particle size on hydrophobic substrate at different time, respectively.

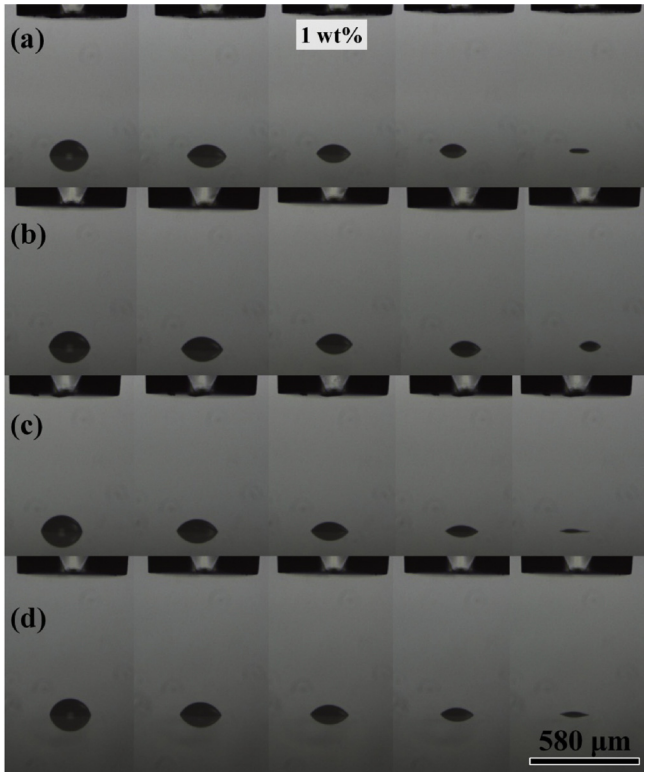

Fig. 9. Deposition images of silica particle solutions (1 wt%, particle concentration) with different particle size ((a) 80 nm, (b) 0.5 μm, (c) 1.0 μm and (d) 1.5 μm) on hydrophobic substrate at different time (0, 510, 1005, 1500 and 2010 μs).

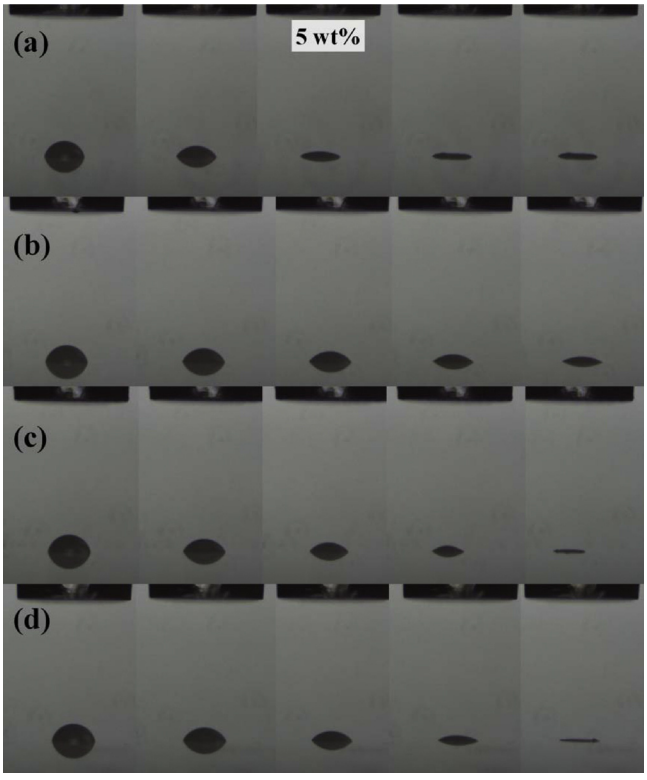

Fig. 10. Deposition images of silica particle solutions (5 wt%, particle concentration) with different particle size ((a) 80 nm, (b) 0.5 μm, (c) 1.0 μm and (d) 1.5 μm) on hydrophobic substrate at different time (0, 510, 1005, 1500 and 1800 μs).

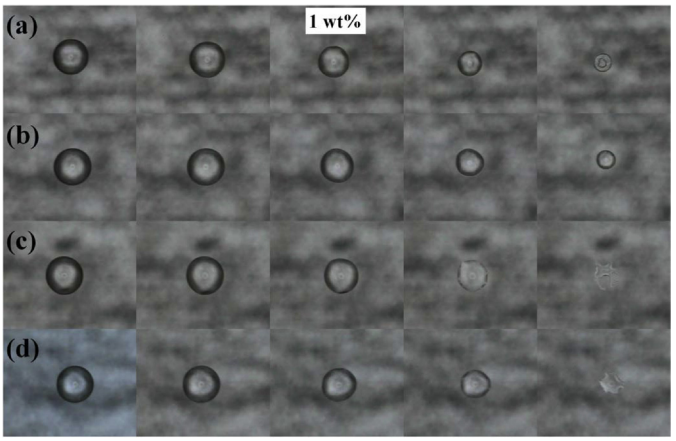

Fig. 11. Top images of the silica particle solutions (1 wt%, particle concentration) with different particle size ((a) 80 nm, (b) 0.5 μm, (c) 1.0 μm and (d) 1.5 μm) on hydrophobic substrate at different time (0, 510, 1005, 1500 and 2010 μs).

All the silica particle solutions exhibited slightly higher shear viscosity than that of the pure solvent [4]. Tuladhar and Mackley reported the slight variation in the shear viscosity of the ink-jet ink fluids with respect to the particle size [22].

The amplitude sweep was examined further to find the linear viscoelastic region before the dynamic oscillation test [11], in which the critical strain was chosen to be 0.14%. As shown in the frequency sweep in Fig. 7, the storage modulus, which describes the slight elastic behavior of the samples [23], increased with increasing angular frequency.

The evaporation properties of the silica solutions-based inks at room temperature were examined and compared by observing the silica solution (1 wt% and 5 wt% particle concentration) drop deposition images on a hydrophobic substrate. The initial volume of the droplet was controlled by the number of droplets jetted from an inkjet head. Jung and Hutchings [24] reported detailed experimental studies on the influences of the impact speed, surface wettability and fluid properties during ink-jet drop deposition.

To obtain the droplet volume and contact angle with respect to time, the side view images were used for image analysis, as shown in Fig. 4 [25]. Fig. 8 shows the drop volume and contact angle changes of the silica particle suspended solutions with different particle sizes, in which the initial volume of the silica solution drop was

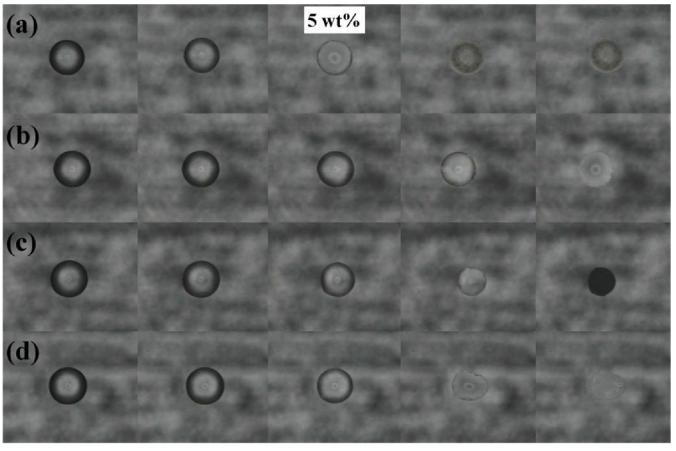

Fig. 12. Top images of the silica particle solutions (1 and 5 wt%, particle concentration) with different particle size ((a) 80 nm, (b) 0.5 μm, (c) 1.0 μm and (d) 1.5 μm) on hydrophobic substrate at different time(0, 510, 1005, 1500 and 1800 μs).

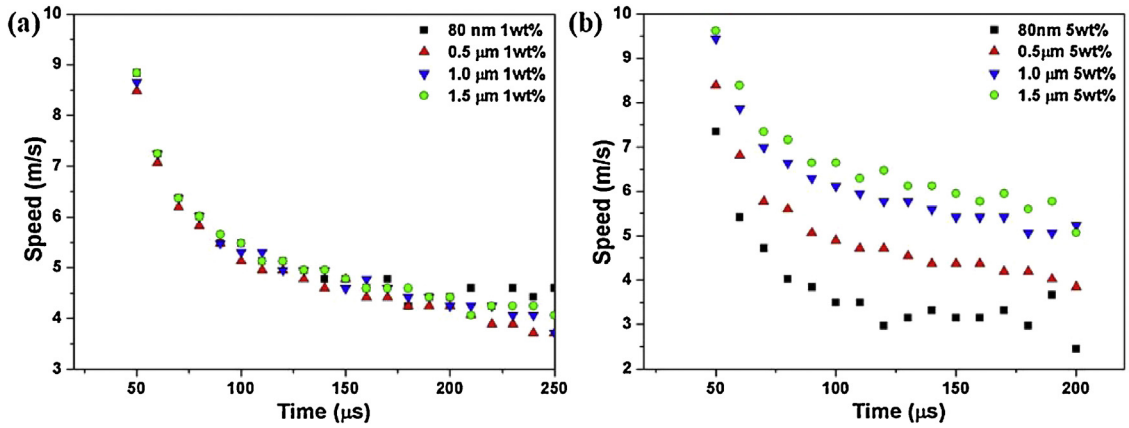

Fig. 13. Jetting speed of the silica particle solutions (1 and 5 wt%, particle concentration).

approximately 2000 pL. Interestingly, the time of the contact angle reaching equilibrium was 80 nm < 1 μm < 1.5 μm < 0.5 μm and the time was shorter at 5 wt% than at 1 wt%. Figs. 9 and 10 show deposition images of a silica solution (1 wt% and 5 wt%, particle concentration). Similarly, from the changes in contact angle shown in Fig. 8, the deposition images of the silica microsphere solutions at 0.5 μm size revealed the slowest decrease in these silica particle solutions at the same time.

Figs. 11 and 12 present top view images of the silica droplets for the 1 and 5 wt% particle concentration, respectively. When the solvent evaporates, only the solid contents remain on the substrate. The size of deposition on the substrate decreased at 1 wt%, whereas a similar size of deposition droplet was obtained at 5 wt%. In addition, an irregular shape of deposition was observed in the microsphere silica particle solutions (1.0 and 1.5 μm) at 1 wt%. Peixinho et al. [26] examined the evaporation and boiling of water confined in the pores of deposits made of mono-dispersed silica colloidal microspheres from a morphological viewpoint. As shown in Figs. 11 and 12, the coffee ring effect was more likely to be observed in case of the evaporation of silica nanoparticle solutions at 1 and 5 wt%.

Studies on the detachment and satellite of the liquid drop are valuable in ink-jetting applications [24,27,28]. The stable drop generation depends on a range of factors including the essential properties of inks and the jetting parameters, such as the applied voltage and pulse width [29,30]. Fig. 13 shows the jetting speed of the silica particle solutions. The methods for obtaining the jetting speed curve during drop formation can be referenced from previous work [18]. The jetting speed of the silica solutions (1 wt%, particle concentration) was approximately 4.33–4.54 m/s in case of the silica solution (5 wt%, particle concentration), and the jetting speed was varied slightly from 3.2 to 5.9 m/s during drop formation.

Fig. 14 presents jetting images of silica particle solutions (1 wt%, particle concentration) at the delay times (40, 70,100, 130, 160, 200, 220 and 250 μs) with an applied voltage of 45 V. Fig. 15 presents jetting images of the silica particle solutions (5 wt%, particle concentration) at various delay times with an applied voltage of 45 V. The jetting performance appeared similar even when the particle size was different in case of a 1 wt% particle concentration. On the other hand, in the case of a higher concentration (5 wt%), the jetting speed (jettability) decreased with decreasing particle size, as shown in Fig. 13(b). This might be related to the increasing shear viscosity with decreasing particle size, as shown in Fig. 6, suggesting that a higher viscosity from a smaller size results in the lower jettability.

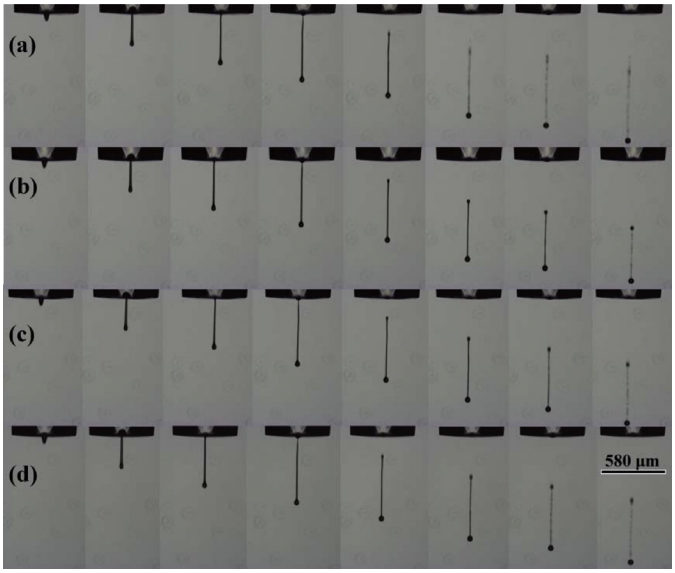

Fig. 14. Jets formed of the silica particle solutions (1 wt%, particle concentration) with different particle size ((a) 80 nm, (b) 0.5 μm, (c) 1.0 μm and (d) 1.5 μm) at 40, 70,100, 130, 160, 200, 220 and 250 μs, respectively with an applied voltage of 45 V.

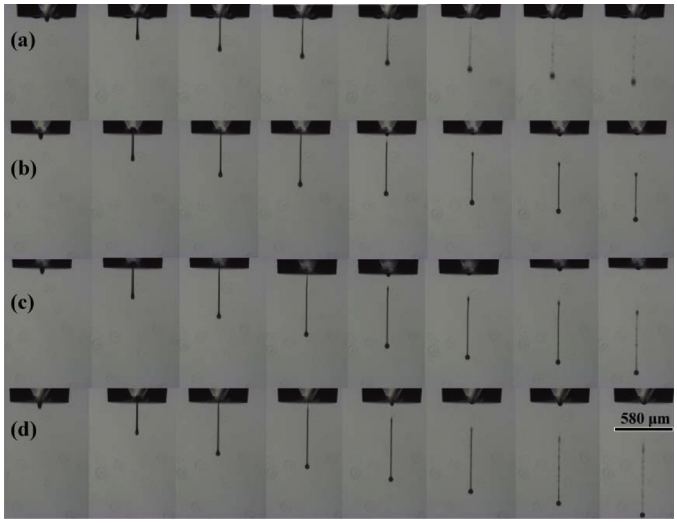

Fig. 15. Jets formed of the silica particle solutions (5 wt%, particle concentration) with different particle size ((a) 80 nm, (b) 0.5 μm (c) 1.0 μm and (d) 1.5 μm) at 40, 70, 100, 120, 140, 160, 180 and 200 μs, respectively with an applied voltage of 45 V.

Conclusions

Silica particle solutions (1 and 5 wt%, particle concentration) with different particle sizes were prepared by dispersing silica particles in ethylene glycol. Their rheological properties were examined using a rotational rheometer, which showed liquid-like properties due to the good dispersibility of silica particles. From experimental studies, the nano-silica solution showed higher viscoelasticity than that of the silica microsphere solutions. A similar deposition size after evaporating the droplets at 5 wt% was observed, whereas a smaller deposition size was detected at 1 wt%. For a silica concentration of 5 wt%, the jetting speed was affected by the size of the silica particle, such that a smaller size particle results in a lower jetting speed due to their higher viscosity.

Acknowledgments

The authors are grateful to Mr. Roh Hyeong Rae for his help on inkjet experiments. K.S. Kwon acknowledges partial support from the Mid-career Research Program through a NRF grant funded by the MEST (NRF-2013R1A2A2A01004802). H.J. Choi acknowledges financial support from the Fundamental R&D Program for Core Technology of Materials funded by the Ministry of Knowledge Economy (K00013-464), Korea.

References

[1] S. Khan, Y.H. Doh, K.H. Choi, A. Khan, N.M. Mohammad, A.A. Gohar, Mater. Manuf. Process. 27 (2012) 1239.
[2] B.W. Jo, A. Lee, K.H. Ahn, S.J. Lee, Mater. Manuf. Process. 26 (2009) 339.
[3] B.J. de Gans, P.C. Duineveld, U.S. Schubert, Adv. Mater. 16 (2004) 203.
[4] S.J. Jung, S.D. Hoath, I.M. Hutchings, Microfluid. Nanofluid. 14 (2013) 163.
[5] K.S. Kwon, Y.S. Choi, D.Y. Lee, J.S. Kim, D.S. Kim, Sens. Actuator A: Phys. 180 (2012) 154.
[6] H.S. Koo, M. Chen, P.C. Pan, Thin Solid Films 515 (2006) 896.
[7] D. Redinger, S. Molesa, S. Yin, R. Farschi, V. Subramanian, IEEE Trans. Electron Devices 51 (2004) 1978.
[8] O. De Los Cobos, B. Fousseret, M. Lejeune, F. Rossignol, M. Dutreilh-Colas, C. Carrion, C. Boissiere, F. Ribot, C. Sanchez, X. Cattoen, M.W.C. Man, J.O. Durand, Chem. Mater. 24 (2012) 4337.
[9] K.J. Fang, S.H. Wang, C.X. Wang, A.L. Tian, J. Appl. Polym. Sci. 107 (2008) 2949.
[10] S. Lee, D. Byun, D. Jun, J. Choi, Y. Kim, J.H. Yang, S.U. Son, S.B.Q. Tran, H.S. Ko, Sens. Actuators A: Phys. 141 (2008) 506.
[11] N. Reis, C. Ainsley, B. Derby, J. Appl. Phys. 97 (2005) 094903.
[12] J. Wu, L. Liu, B. Jiang, Z. Hu, X.Q. Wang, Y.D. Huang, D.R. Lin, Q.H. Zhang, Appl. Surf. Sci. 258 (2012) 5131.
[13] B.J. Park, B.O. Park, B.H. Ryu, Y.M. Choi, K.S. Kwon, H.J. Choi, J. Appl. Phys. 108 (2010) 102803.
[14] D. Xu, V. Sanchez-Romaguera, S. Barbosa, W. Travis, J. de Wit, P. Swan, S.G. Yeates, J. Mater. Chem. 17 (2007) 4902.
[15] S.D. Hoath, O.G. Harlen, I.M. Hutchings, J. Rheol. 56 (2012) 1109.
[16] X.X. Wang, Y.J. Yin, C.X. Wang, Colloids Surf. A: Physicochem. Eng. Asp. 361 (2010) 51.
[17] B. Scheid, J. Delacotte, B. Dollet, E. Rio, F. Restagno, E.A. van Nierop, I. Cantat, D. Langevin, H.A. Stone, EPL 90 (2010) 24002.
[18] K.S. Kwon, J. Micromech. Microeng. 20 (2010) 115005.
[19] S.D. Hoath, I.M. Hutchings, G.D. Martin, T.R. Tuladhar, M.R. Mackley, D. Vadillo, J. Imaging Sci. Technol. 53 (2009) 041208.
[20] N.F. Morrison, O.G. Harlen, Rheol. Acta 49 (2010) 619.
[21] H. Yoo, C. Kim, Rheol. Acta 52 (2013) 313.
[22] T.R. Tuladhar, M.R. Mackley, J. Non-Newton. Fluid Mech. 148 (2008) 97.
[23] D.C. Vadillo, T.R. Tuladhar, A.C. Mulji, M.R. Mackley, J. Rheol. 54 (2010) 781.
[24] S. Jung, I.M. Hutchings, Soft Matter 8 (2012) 2686.
[25] K.S. Kwon, S.H. An, M.H. Jang, J. Korean Soc. Precis. Eng. 30 (2013) 414.
[26] J. Peixinho, G. Lefevre, F.X. Coudert, O. Hurisse, J. Colloid Interface Sci. 408 (2013) 206.
[27] C. Wagner, Y. Amarouchene, D. Bonn, J. Eggers, Phys. Rev. Lett. 95 (2005) 164504.
[28] S.D. Hoath, S.J. Jung, W.K. Hsiao, I.M. Hutchings, Org. Electron. 13 (2012) 3259.
[29] A.K. Mogalicherla, S. Lee, P. Pfeifer, R. Dittmeyer, Microfluid. Nanofluid. 16 (2014) 655.
[30] S.D. Hoath, W.K. Hsiao, S. Jung, G.D. Martin, I. Hutchings, N.F. Morrison, O.G. Harlen, J. Imaging Sci. Technol. 57 (1) (2013) 10503-1.